

Metallic gold slows disease progression, reduces cell death and induces astrogliosis while simultaneously increasing stem cell responses in an EAE rat model of multiple sclerosis

Dan Sonne Pedersen · Pil Møntegaard Fredericia · Mie Østergaard Pedersen · Meredin Stoltenberg · Milena Penkowa · Gorm Danscher · Jørgen Rungby · Agnete Larsen

Accepted: 10 May 2012
© Springer-Verlag 2012

Abstract Multiple sclerosis (MS) is the most common neurodegenerative disease in the Western world affecting younger, otherwise healthy individuals. Today no curative treatment exists. Patients suffer from recurring attacks caused by demyelination and underlying neuroinflammation, ultimately leading to loss of neurons. Recent research shows that bio-liberation of gold ions from metallic gold implants can ameliorate inflammation, reduce apoptosis and promote proliferation of neuronal stem cells (NSCs) in a mouse model of focal brain injury. Based on these findings, the present study investigates whether metallic gold implants affect the clinical signs of disease progression and the pathological findings in experimental autoimmune encephalomyelitis (EAE), a rodent model of MS. Gold particles 20–45 µm suspended in hyaluronic acid were bilaterally injected into the lateral ventricles (LV) of young Lewis rats prior to EAE induction. Comparing gold-treated animals to untreated and vehicle-treated ones, a statistically significant slowing of disease progression in terms of reduced weight loss was seen. Despite massive inflammatory infiltration, terminal deoxynucleotidyl transferase dUTP nick end labeling staining revealed reduced

apoptotic cell death in disease foci in the brain stem of gold-treated animals, alongside an up-regulation of glial fibrillary acidic protein-positive reactive astrocytes near the LV and in the brain stem. Cell counting of frizzled-9 and nestin-stained cells showed statistically significant up-regulation of NSCs migrating from the subventricular zone. Additionally, the neuroprotective proteins Metallothionein-1 and -2 were up-regulated in the corpus callosum. In conclusion, this study is the first to show that the presence of small gold implants affect disease progression in a rat model of MS, increasing the neurogenic response and reducing the loss of cells in disease foci. Gold implants might thus improve clinical outcome for MS patients and further research into the long-term effects of such localized gold treatment is warranted.

Keywords Dissolucytosis · EAE · Inflammation · Metallic gold · Neural stem cells

Introduction

Multiple sclerosis (MS) is the most common non-traumatic neurodegenerative disease in the Western world, affecting mainly young adult individuals (Trapp and Nave 2008). Although the severity of this chronic disease varies, many patients experience increasing physical immobility (Love et al. 2008, p. 1516) and often cognitive functions are also slowed during MS (Achiron et al. 2007), adding to the mental stress of the patients. Additionally, more than half of all MS patients suffer from depression (Trapp and Nave 2008), which might correlate to a reduced hippocampal volume and cortisol hypersecretion in MS patients (Sicotte et al. 2008; Caetano et al. 2004; Gold et al. 2010). MS develops as a response to a complex pattern of genetic

D. S. Pedersen (✉) · M. Stoltenberg · G. Danscher · J. Rungby · A. Larsen
Department of Biomedicine, Pharmacology,
Aarhus University, Wilhelm Meyers Allé 4,
Building 1240, 3rd Floor, 8000 Aarhus C, Denmark
e-mail: dspe@farm.au.dk

D. S. Pedersen · P. M. Fredericia · M. Ø. Pedersen · M. Penkowa
Department of Neuroscience and Pharmacology,
University of Copenhagen, 2200 Copenhagen, Denmark

G. Danscher
Berlock ApS, Gentoftvej 7, 8000 Aarhus C, Denmark

traits (McFarland and Martin 2007) interacting with a series of environmental factors (Giovannoni and Ebers 2007) and ultimately resulting in ongoing autoimmune inflammation causing widespread demyelination and irreversible nerve cell death (McFarland and Martin 2007). As of today, no cures exist but there are increasing attempts to use conventional immunosuppressive agents to slow the progression of MS (Drachman and Brodsky 2005).

Gold salts are among the oldest known immune suppressives and have been used in the treatment of rheumatoid arthritis since the early twentieth century (Forestier 1934; Williams 1935). Clinical use of gold salts have, however, been limited due to the systemic spread of gold ions causing adverse effects, such as nephrotoxicity, necessitating close monitoring of patients when applying traditional gold treatments (Schiff and Whelton 2000). However, in 2002, Danscher showed that metallic gold implants could be used as an alternative source of gold, releasing gold ions into the surrounding tissue (Danscher 2002). This bio-liberation of gold ions, termed dissolutocytosis, is a slow and highly localized macrophage-induced, extracellular liberation of gold ions from non-phagocytizable gold pieces, (i.e., $>20\ \mu\text{m}$) resulting in an extremely limited systemic spreading of gold ions to other organs (Danscher 2002). Bio-liberated gold ions exhibited powerful, anti-inflammatory properties in a mouse model of traumatic brain trauma injury (TBI) markedly reducing microgliosis, oxidative stress and neuronal apoptosis when injecting small gold implants prior to trauma (for a review, see Danscher and Larsen 2010).

Though limited to distinct areas (Robel et al. 2011), lifelong neurogenesis is of great importance for functioning of the adult brain (Ge et al. 2007; Deng et al. 2009) and evidence accumulates, showing that the activity of the immune system plays a key role in the regulation of adult neurogenesis from the neurogenic niches (Gonzalez-Perez et al. 2010); thus, an increased neurogenesis might constitute an endogenous defense against demyelination and neuron loss. Interestingly, bio-liberated gold ions also resulted in increased NSC proliferation in the murine TBI model (Larsen et al. 2008), although it has not been presently unraveled if gold has a direct effect on NSCs or if the regenerative processes occur in response to a gold induction modification of the inflammatory response to lesions.

The present study investigates whether an MS model, i.e., experimental autoimmune encephalomyelitis (EAE), could benefit from treatment with metallic gold. Both clinical signs of disease, i.e., the extent of paresis and histopathological signs of disease and neuroregeneration, were examined. Clinically, we found a statistical slowing of disease progression (paresis/paralysis) accompanied by a reduction in disease-related weight loss. Histopathologically, we saw signs of neurogenesis and neuroprotection,

though no direct reduction in macrophage/microglia activation and lymphocyte involvement was evident.

Materials and methods

Animals

A total of 48 female Lewis rats, 2 months old and weighing approximately 200 g (Charles River, Germany), were used for this study. The animals were kept under standardized conditions of light and temperature, with a 12-h day/night cycle and had free access to food and water. The animals were divided into four groups of 12 animals. Groups no. 3 and 4 were treated with either hyaluronic acid (HA) or metallic gold particles suspended in HA, respectively, 17 days prior to EAE immunization. After the animals had recovered fully from the treatment procedures, group 2, 3 and 4 were EAE immunized (day zero). All animals were weighed and scored clinically on a daily basis. During progression of EAE, leading to motor disabilities, animals had water in a Petri dish and soaked chow for easy intake to ensure sufficient intake of liquid and nutrients. The healthy animals were used as comparison and control of the EAE exposed animals. All animal experiments were conducted in accordance with the ethical guidelines of the University of Copenhagen and approved by the Animal Experiments Inspectorate, controlled by The Danish Ministry of Justice.

Gold treatment

The procedures for gold treatment have previously been described in detail (Larsen et al. 2008). As much as 463 mg of 99.9 % pure metallic spherical gold particles, 20–45 μm in size (Alfa-Aesar, Karlsruhe, Germany), were mixed with 0.85 mL of sodium HA (10 mg/mL, ProVisc, Alcon, SE). After being anaesthetized, the rats were placed in a stereotaxic instrument (ANY-Angle, 51400, Stoelting Co, USA) and a total of 20 μL (10 μL in each hemisphere) of gold–HA mixture or pure HA was injected bilaterally in the LVs of the brain using Hamilton syringes (Microliter, #702, Switzerland). On both sides, injections were placed 3.2 mm from the surface at the following coordinates: 0.8 mm posterior and 1.4 mm lateral from the bregma (Paxinos and Watson 1986). Animals received analgesic treatment (Temgesic, Reckitt & Colman, Hull, UK, 0.3 mg/kg) for 2 days following the stereotaxic surgery. The gold and placebo treatments were given 17 days prior to the induction of EAE.

EAE induction

EAE was induced by intradermal (i.d.) injection of 0.2 mL of an emulsion consisting of 100 μg Myelin Basic Protein

(MBP) from guinea pig (Sigma, USA, M2295) suspended in 0.1 mL of saline (0.9 %) and 0.1 mL complete Freund's adjuvant (CFA; Difco, USA, 0638), with the addition of 0.2 µg of Mycobacterium Tuberculosis H37 Ra (Difco, USA, 3114). This emulsion was given intradermally at the base of the tail of each rat in the EAE control, placebo and gold-treated groups under Isoflurane anesthesia (Isoflurane Baxter, Baxter, USA, KDG9623).

Score of clinical symptoms

The animals were monitored daily, weighed and clinically scored according to the following scale (Imrich and Harzer 2001): 0, no clinical signs of EAE; 1, loss of tail tonus; 2, mild paresis in one or both hindlimbs; 3, moderate paresis in one or both hindlimbs; 4, severe paresis or paralysis in one or both hindlimbs; 5, paralysis in one or both hindlimbs and visible paresis in one or both forelimbs, incontinence; 6, moribund. No animal was permitted to lose more than 20 % bodyweight (compared to the starting point of EAE immunization) just as no animals were allowed to go beyond score 4; thus, as the animals reached score 4 by day 10, the animals were anaesthetized and killed by transcardial perfusion. Weight measurements were done, as weight loss serves as an important clinical sign of illness in animals (Wisikin et al. 2010).

Tissue processing

The rats were deeply anaesthetized with 0.2 mL/100 g Hypnorm®/Dormicum® s.c. and transcardially perfused with 0.9 % saline containing 0.3 % heparin (15,000 IU/L) for 1 min followed by Zamboni's fixative (2 % paraformaldehyde, 15 % picric acid in 0.1 M sodium phosphate buffer with pH 7.4) for 8–10 min. After perfusion, the brains were immediately removed and allowed to postfixate for 4 h. The fixed brains were divided sagittally through the midline, dehydrated and embedded in paraffin before the right hemisphere was selected for slicing into 8-µm thick sagittal sections.

Selection of sections for staining

Sections including the brain stem were matched from different treatment groups to include identical anatomical structures in the brain stem and ventricular system. Specifically, sections were chosen when including structures defined in the Atlas of the Rat Brain (Paxinos and Watson 1986), Figs. 80–84 (i.e., all sections included comparisons of the LVs, hippocampus, brain stem and cerebellum). Matching of sections was ensured by the morphology of these structures. A series of matched sections from the three groups, EAE, EAE vehicle treated and EAE gold-

treated, were randomly chosen for each staining. Occasionally, anatomically matching sections were not available from all animals due to technical reasons, but each series comprised successfully stained and matching sections from at least eight different animals from each group.

Autometallography

100 mL of autometallography (AMG) developer was made of 60 mL gum arabic solution (Bidingen, DK) to which was added 10 mL of sodium citrate buffer [25.5 g of citric acid (Merck, 0244 supplied by VWR, DK), 23.5 g sodium citrate (Merck 6448, VWR, DK)] to 100 mL distilled H₂O, 15 mL of reducing agent [0.85 g of hydroquinone (Merck 4610, VWR, DK) dissolved in 15 mL distilled water at 40 °C] and 15 mL of solution containing silver ions [0.12 g silver lactate (Fluka 85210 supplied by Sigma-Aldrich, DK) in 15 mL distilled water at 40 °C]. The AMG developer was prepared immediately before use, thoroughly stirred and placed in a jar in a 26 °C water bath. Tissue slices were placed in the jar under a dark hood and developed for 60 min. Afterward, the AMG development was stopped by replacing the developer with a 5 % thio-sulfate solution for 10 min. Finally, the sections were rinsed several times in distilled water, counterstained and lastly mounted for light microscopy. The AMG process has been described in detail by (Danscher and Stoltenberg 2006).

Histochemistry

Tissue preparation for histochemistry and immunohistochemistry analyses

Paraffin sections were rehydrated according to standard procedures (3 × 5 min in xylene, 2 × 5 min in 99 % alcohol, 1 × 2 min in 96 % alcohol and 1 × 2 min in 70 % alcohol), and if necessary subjected to heat-induced epitope retrieval (HIER) in citrate buffer with pH 6.0 for 10 min (nestin). The sections were then incubated in 1.5 % H₂O₂ in Tris-buffered saline (TBS)/Nonidet (TBS: 0.05 M Tris, pH 7.4, 0.15 M NaCl, with 0.01 % Nonidet P-40) (Sigma-Aldrich, USA, N-6507) for 20 min at room temperature to quench endogenous peroxidase, followed by incubation in 10 % goat serum (In Vitro, DK, 04009-1B) in TBS/Nonidet for 30 min at room temperature to block nonspecific binding. After these steps, the sections were ready for histochemistry and immunohistochemistry.

Hematoxylin–eosin

Hematoxylin–eosin (HE) staining of brain sections was performed in accordance with standard procedures. In

short, the slides were deparaffinized, rinsed under tap water for 10 min, and then incubated 10 min in hematoxylin, followed by rinsing under tap water for another 10 min. Next, the slides were incubated in eosin for 3–4 min before dehydration in ethanol and mounted with cover slides. The HE staining was used to validate one of the hallmarks of EAE pathology, i.e., a high degree of infiltration of peripheral mononuclear immune cell immune cell (Hickey et al. 1983). These were identified as small, round, dense and bluish colored cells, especially in parenchymal cuffs surrounding the blood vessels.

Lectin

Sections were incubated overnight at 4 °C with biotinylated tomato lectin from *Lycopersicon esculentum* (Sigma-Aldrich, USA, L9389, 1:500), used as a marker for microglial cell populations. Lectin stains both activated and resting microglia, and macrophages as well (Acarin et al. 1994). Lectin was developed using streptavidin–biotin-peroxidase complex (StreptABComplex/HRP, Dako, DK, K377), prepared according to the manufacturer's recommended dilutions, for 30 min at room temperature. The lectin staining was visualized by adding 0.015 % H₂O₂ to 3,3'-diaminobenzidine (DAB) dissolved in Milli-Q water (1 mg/mL)(Millipore Reference, Germany) for 10 min at room temperature (RT).

Terminal deoxynucleotidyl transferase dUTP nick end labeling staining

The sections were deparaffinized and incubated with 20 µg/mL proteinase K (Sigma) for 5 min to strip off nuclear proteins. Terminal deoxynucleotidyl transferase dUTP nick end labeling (TUNEL) was accomplished using the Apoptag Plus in situ apoptosis detection kit (Oncor, Gaithersburg, US, S7101-KIT) according to the manufacturer's instructions. After immersion in equilibration buffer for 10 min, sections were incubated with TdT and dUTP-digoxigenin in a humidified chamber at 37 °C for 1 h and then incubated in the stop–wash buffer at 37 °C for 30 min to stop the reaction. After washing in PBS buffer, the sections were incubated in anti-digoxigenin peroxidase solution for 30 min. Afterward, apoptotic cells were visualized by adding 0.015 % H₂O₂ to DAB dissolved in Milli-Q water (1 mg/mL) for 10 min at RT, and finally the sections were counterstained with toluidine blue.

Immunohistochemistry

Sections were incubated overnight at 4 °C with the following primary antibodies: rabbit anti-cow glial fibrillary acidic protein (GFAP), a marker of reactive astrocytes (Dako, DK, Z334, 1:250); rabbit anti-human frizzled-9, a marker of NSCs (Abcam, UK, Ab13000, 1:100); mouse anti-rat nestin, a marker of stem cells and reactive

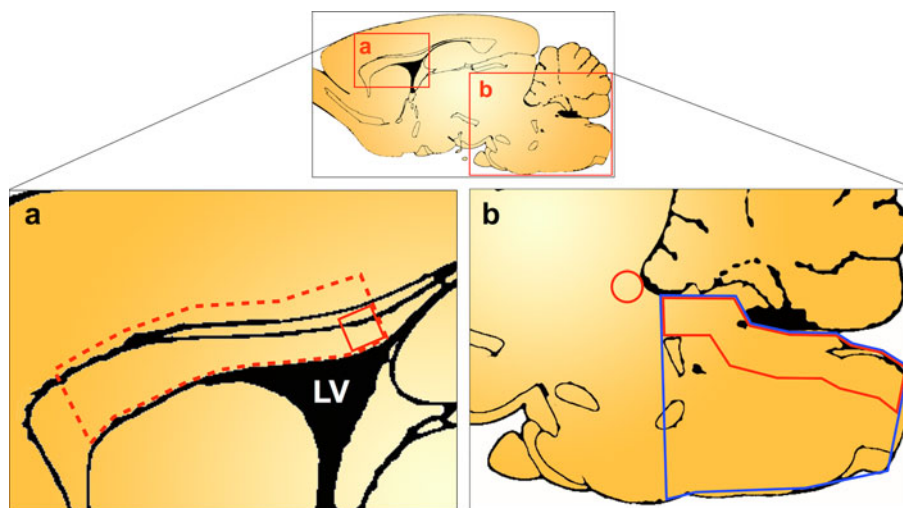


Fig. 1 Overview over areas counted, modified from Paxinos and Watson's Atlas of the Rat Brain (Paxinos and Watson 1986), from which Fig. 83 was chosen as representative for Figs. 80–83. Thus, the shown areas are not precise but denote the approximate location of the areas chosen for evaluation and counting of positive cells. The small panel gives an overview over the two main areas of interest, i.e., the SVZ (a) and brain stem (b), in which protein expressions were

evaluated. **a** The dashed line box denotes the counting area of frizzled-9, nestin and MT-1 and -2. The small square denotes the GFAP counting area. **b** Small circle denotes second GFAP counting area, while the blue area denotes counting of apoptotic cells. The red rectangular area was used for counting of microglia. LV lateral ventricle

astrocytes (Chemicon, Billerica, US, MAB353, 1:200); metallothionein-1 and -2 (MT-1 and -2), a neuroprotective metalloprotein (Dako, DK, M0639, 1:50); mouse anti-rat CD3, a marker of all types of T cells or NK cells (Serotec, UK, MCA 772).

On the second day, the primary anti-body was detected using biotinylated secondary antibodies (anti-mouse IgG, Sigma-Aldrich, USA, 8774, diluted 1:200 for nestin and MT-1 and -2 staining; anti-rabbit IgG, Sigma-Aldrich, USA, 3275, diluted 1:400 for GFAP and frizzled-9 staining; goat anti-mouse IgG, Jackson, US, 115-065-020, diluted 1:10 for CD3), incubating for 30 min at room temperature. All staining were enhanced using streptavidin-biotin peroxidase complex (StreptABComplex/HRP, Dako, DK, code K377) and tyramide signal amplification (TSA)-kit (NEN, Life Science Products, US, NEL700A), which were both applied following the manufacturer's recommendations. Finally, the immune reactions were visualized by using 0.015 % H₂O₂ in 5 mL DAB dissolved in Milli-Q water (1 mg/mL) for 10 min at RT.

Identification and counting of cells

Lectin

Microgliosis was identified by means of microglial morphology, as they retract their processes, shifting from resting to reactive microglia and ending up practically void of processes. Using anatomically matched sections of the brain stem, the number of reactive microglia was counted at 40× magnification within an area representing the apparent highest density of positive cells in the dorsal part of the brain stem (Fig. 1b).

CD3+

Infiltrating mature T cells positive for the CD3+ marker, required for their activation (Doucey et al. 2003), were identified by a small, round and densely colored morphology, resembling active microglia. The number of cells was systematically counted in the brain stem at 40× magnification, using anatomically matched sections (Fig. 1b).

Terminal deoxynucleotidyl transferase dUTP nick end labeling

Positive cells were identified as cells in which the nuclei were dense and intensely and dark-brownish colored due to the staining of processes taking place in the beginning of apoptosis. Using anatomically matched sections, the number of cells was systematically counted at 40× magnification using neighboring microscopic fields until the whole area of the brain stem had been covered (Fig. 1b).

Glial fibrillary acidic protein

The numbers of GFAP positive and reactive astrocytes were evaluated by counting at 20× magnification at two locations (Fig. 1a, b) and matched throughout the animals: one area subventricular, above the LVs and the adjacent part of the corpus callosum (CC); the second area at the caudal part of the dorsal mesencephalic tegmentum near the fourth ventricle. Astrocytes were considered positive when displaying a hypertrophic soma, i.e., dense and large, with retracted, thickened processes.

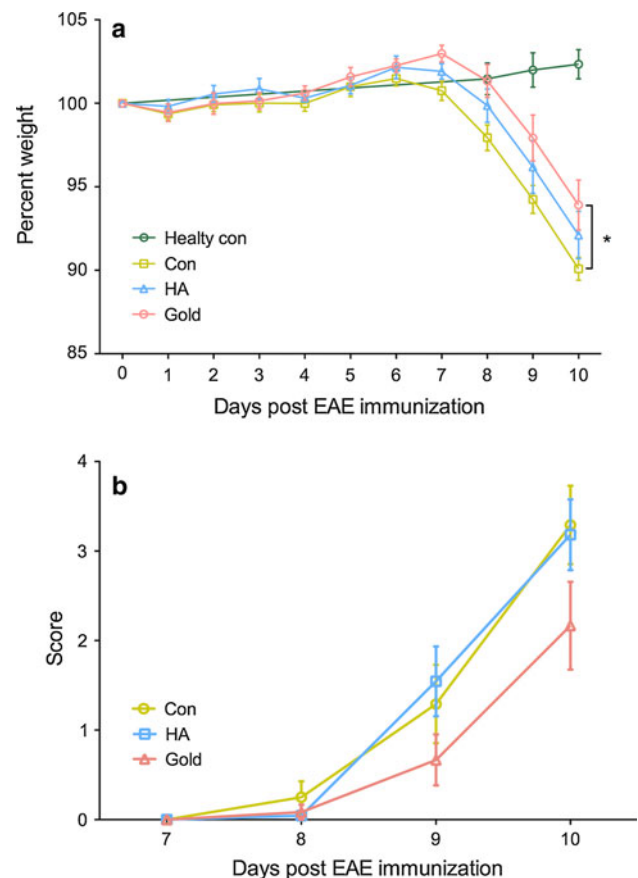


Fig. 2 **a** Course of weight loss during development of experimental autoimmune encephalomyelitis (EAE) normalized in percentage to day 0, in which the EAE emulsion was injected. Except for the healthy controls, which gained weight as expected, all animals had lost considerable weight on day 10 compared to day 0. The gold-treated group did, however, begin to lose weight 1 day later than the vehicle group and in addition less weight loss was seen in the gold-treated animals. Analysis of day 10 weight data by the Student's *t* test revealed a statistically significant difference between the EAE control and gold-treated group ($P = 0.035$). **b** The clinical symptoms of EAE developed from day 8 and showed a sharp increase during the next 2 days, topping at day 10; however, no statistically significant difference was found in comparison of the gold-treated group with the control groups

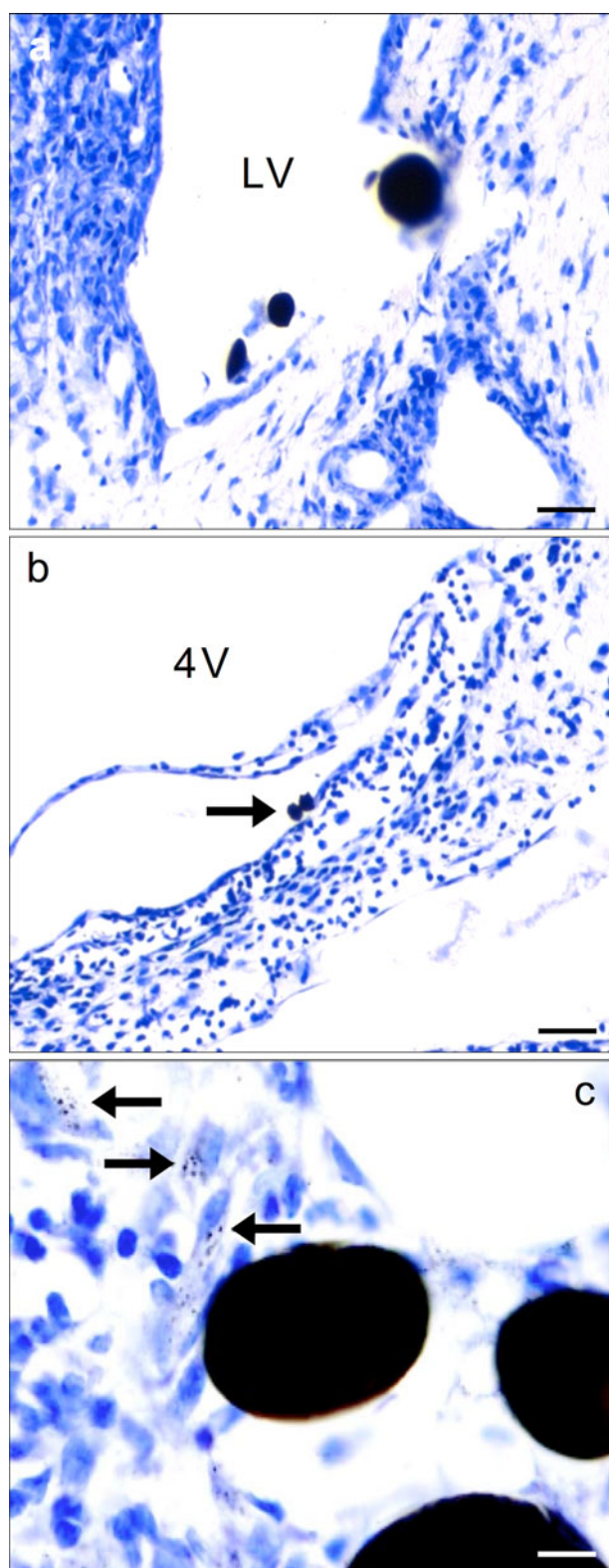


Fig. 3 Tracing of silver-enhanced gold ions by AMG and visualized by light microscopy. **a, b** The uptake of gold ions in cells near the injected gold, shown by the *arrow* in both pictures. **c** Gold-loaded cells are seen in close proximity to the gold particles. *Scale bars* 20 μ m. *Scale bars* 50 μ m (**a**) and 10 μ m (**c**)

Frizzled-9

The response of NSCs was evaluated using the marker frizzled-9 and was studied in the subventricular zone (SVZ) and neighboring parts of CC. Frizzled-9-positive cells were counted at 40 \times magnification (Fig. 1a). Positive cells were identified as exhibiting a fuzzy, undifferentiated morphology, being lightly colored and with no, or only minor, processes.

Nestin

Nestin-positive cells, considered a marker of neural progenitor cells (Michalczyk and Ziman 2005; Wiese et al. 2004), were seen as densely colored and hypertrophic soma with small thick processes. The numbers of nestin-positive and thus proliferating cells were evaluated by counting at 40 \times magnification at two locations, i.e., next to the LV and rostrally to LV, from which the mean cell count was calculated (Fig. 1a).

Metallothionein-1 and -2

Morphologically, metallothionein-1 and -2 (MT-1 and -2) positive cells appeared with the shape of reactive astrocytes, displaying a densely colored and almost round soma with a nearly complete retraction of processes. The number of MT-1 and -2 positive cells was counted at 40 \times magnification within three foci presenting the highest density of positive cells, i.e., rostrally to LV, in CC adjacent to SVZ, and above the hippocampal area, above LV and (Fig. 1a). Mean cell counts from within the three foci were calculated.

Morphological disease evaluation and cell counting procedures

Histopathologically, EAE is known to be a widespread disease causing infiltration of lymphocytes and macrophages/microglia in various disease foci throughout the brain, but with a preference for the brain stem and periventricular areas. The inflammatory infiltrates are known to be located in the perivascular areas, sometimes spreading deeper into the surrounding tissue as the disease progresses (Love et al. 2008, p. 1525; Holman et al. 2010). Thus, the main focus was directed against the periventricular areas. All staining was evaluated in terms of anatomical localization and the morphological characteristics of the positively stained cells. The numbers of positive cells were quantified by means of blinded cell counting. These were carried out at either 20 \times (480 \times 480 μ m) or 40 \times (250 \times 250 μ m) magnifications, using a Zeiss AxioStar Plus (Carl Zeiss, Germany) microscope, equipped with a graticule, i.e., numbered grid (Pyser-SGI Ltd, NE11A \varnothing 26 mm, UK),

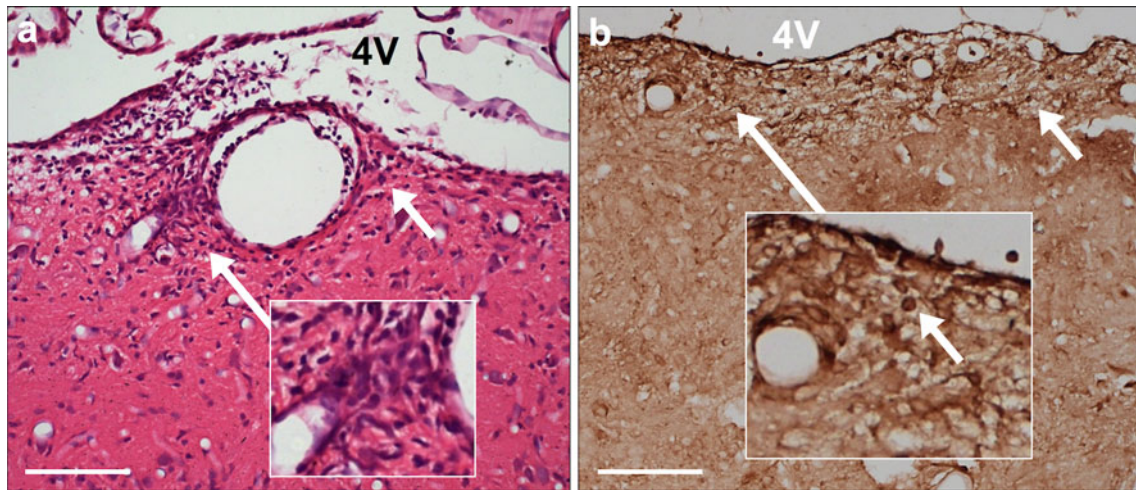


Fig. 4 Micrographs of stainings with hematoxylin–eosin (HE) and anti-CD3 antibody. **a** HE staining showing massive infiltration of mono- and lymphocytes from circulation, giving rise to pronounced vascular cuffs, as confirmation of a strong EAE induction. *Arrows*

denote infiltrating cells. **b** CD3-positive cells, a marker of types of mature CD4 and CD8 T cells, also show active, inflammatory cells. *Insets* are digitally enlarged. *Scale bars* 100 μm

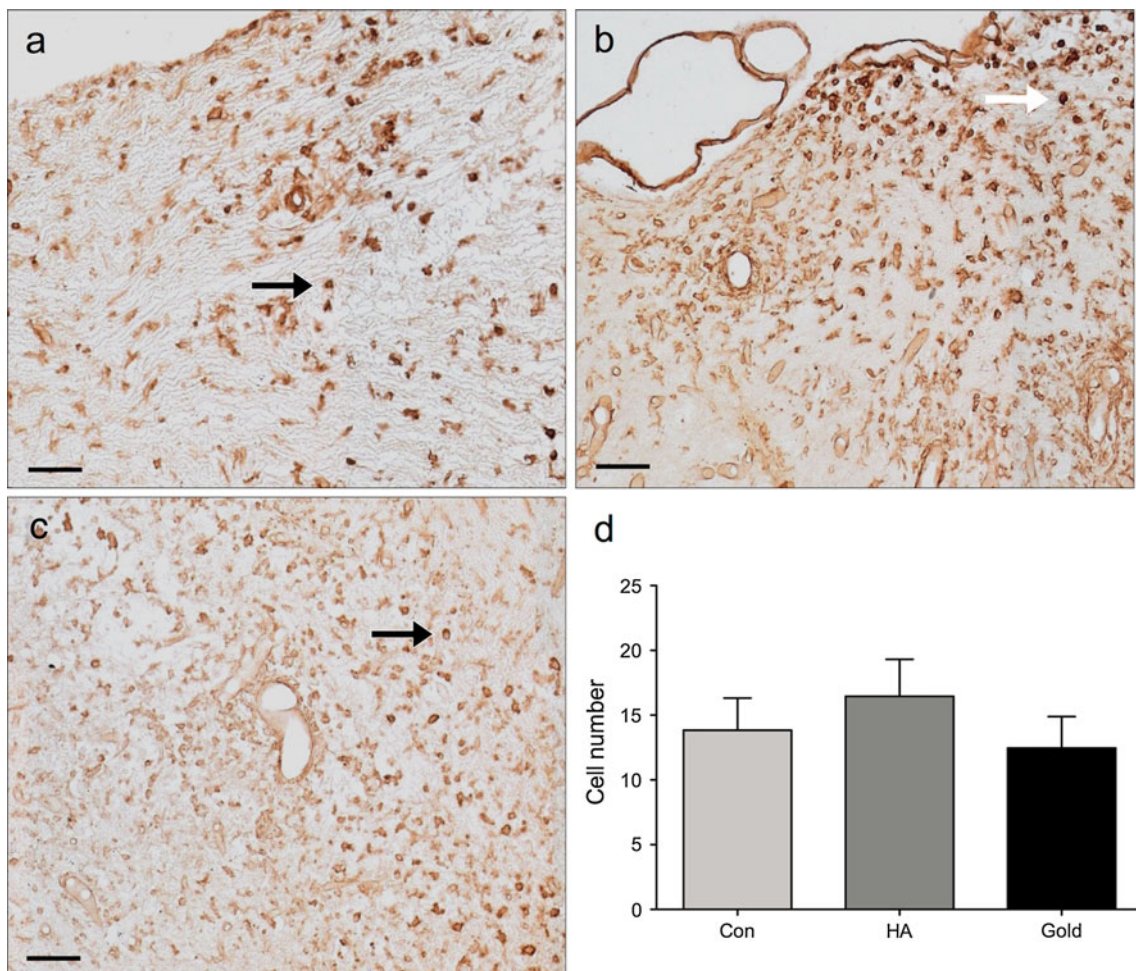


Fig. 5 Micrographs of microglia are shown, as expressed by lectin staining. **a–c** The *arrows* in micrographs show reactive microglia in the brain stem. **d** Counting of microglia in infiltrated areas, i.e., hot spots did not reveal any significant differences ($P > 0.05$). *Scale bars* 100 μm

on all countings. The areas chosen for counting are illustrated in Fig. 1, which is representative for Figs. 80–84 in Paxinos and Watson's Atlas of the Rat Brain (Paxinos and Watson 1986).

Statistical calculations

Weight data were normalized to day 0, and data from day 10, the day of disease peak, were analyzed using Student's *t* test. Clinical scores on day 10 as well as the total score obtained on day 7–10 were analyzed using the Mann–Whitney rank sum test. For histology, positive cells in the brain sections were counted in at least eight ($n = 8–10$) animals from each group, varying due to technical reasons identified prior to counting. The mean values were calculated and the effect of gold treatment versus the vehicle on EAE was evaluated using Student's *t* test. In all tests the level of statistical significance was $P < 0.05$.

Results

Clinical evaluation

Out of 48 animals, 36 underwent EAE immunization, all of which became ill and displayed clinical symptoms of the disease as early as day 7 after immunization, i.e., 100 % disease induction was obtained in all groups. The animals started displaying symptoms of clinical illness already at day 7 post EAE immunization, indicating a strong induction of EAE in our experimental setup, and at day 10, when the first animals reached a disease level equivalent to score 4, all animals were killed.

Disease progression after gold treatment

The healthy control animals gained weight as expected during the experimental period, whereas the EAE groups lost weight due to their illness. As depicted in Fig. 2a, the

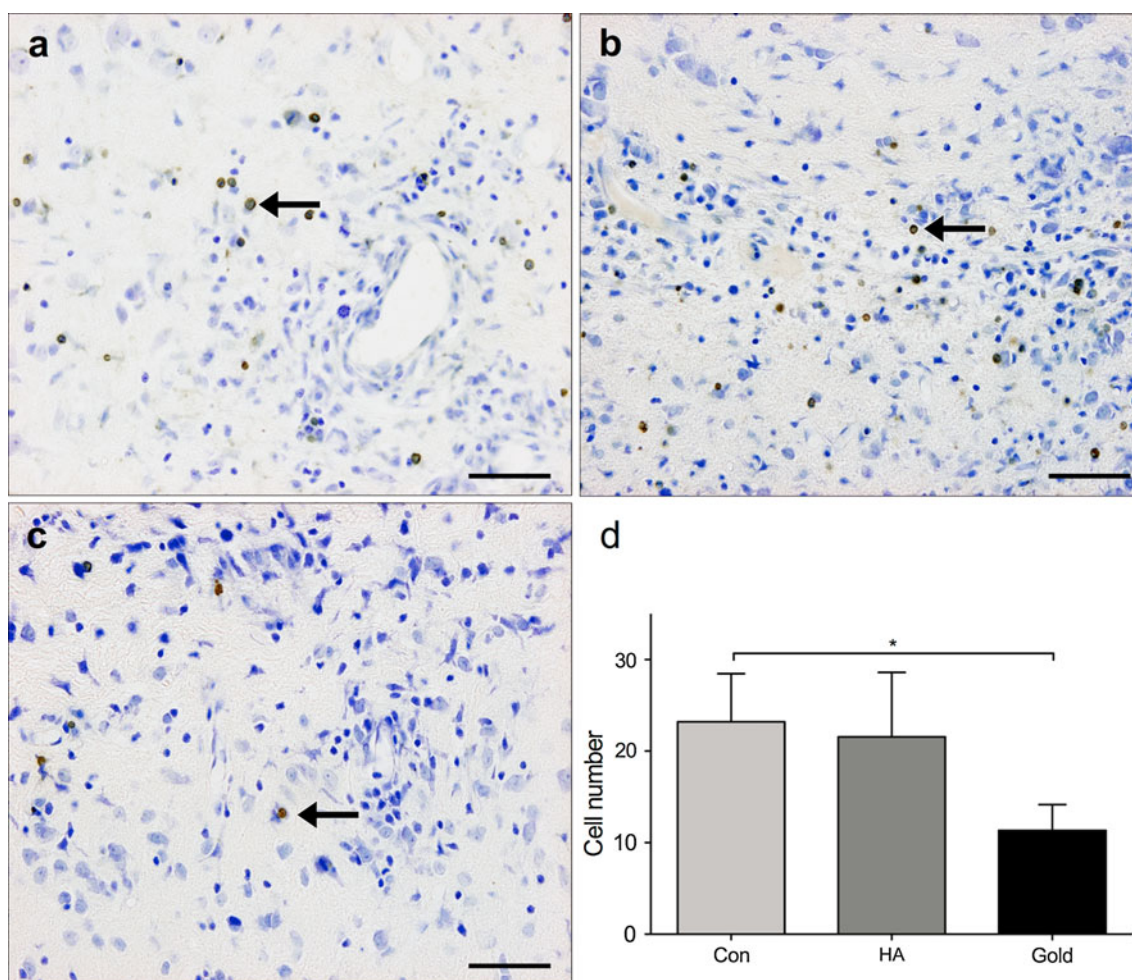


Fig. 6 Micrographs showing the amount of TUNEL-positive cells in the brain stem and cell count of positive cells. **a–c** The arrow denotes a TUNEL-positive cell. **d** A significant reduction in cell death was

seen in the gold-treated animals, compared to the control group. Scale bars 50 μm

overall EAE-induced weight loss was significantly lower at disease peak (day 10) in the gold-treated group ($93.9 \pm 1.5\%$) compared to the EAE control ($90.1 \pm 0.7\%$) ($P = 0.03$). Supporting this finding, the clinical score of the gold-treated animals also exhibited a tendency to decline (Fig. 2b), as the average overall score, i.e., sum of score points registered at day 7–10, were 2.9 in the gold-treated group compared to 4.8 ($P = 0.11$) in the EAE group and 4.7 in the HA-treated group respectively. Looking at disease peak alone, the average score per animal was 2.2 in the gold group compared to 3.3 in the EAE group ($P = 0.09$) and 3.2 in the HA group.

Gold tracing

The injected gold particles had spread through the ventricular system and gold particles were found also in the fourth ventricle (Fig. 3b). AMG confirmed that there was

dissolucytotic liberation of gold ions from the implanted metallic gold particles, accumulating in the cytoplasm of the cells, although the gold staining was rather small and mostly confined to periventricular tissues (Fig. 3a–c). Traces of gold ions were seen in both neurons and glia cells, accumulating in the cytoplasm of the cells.

Gold implants have no observable effects on macrophage/microglia and lymphocyte infiltration

Overall, HE histology revealed a high amount of infiltrating immune cells, serving as evidence of a solid induction of EAE in the rats (Fig. 4a). The observed pathological changes showed a high degree of inflammation and infiltration in all three experimental groups with no apparent difference between the groups. Likewise, CD3 positive cells i.e., CD4 and CD8 cells of T-lineage (Olson et al. 2004) were quantified by means of

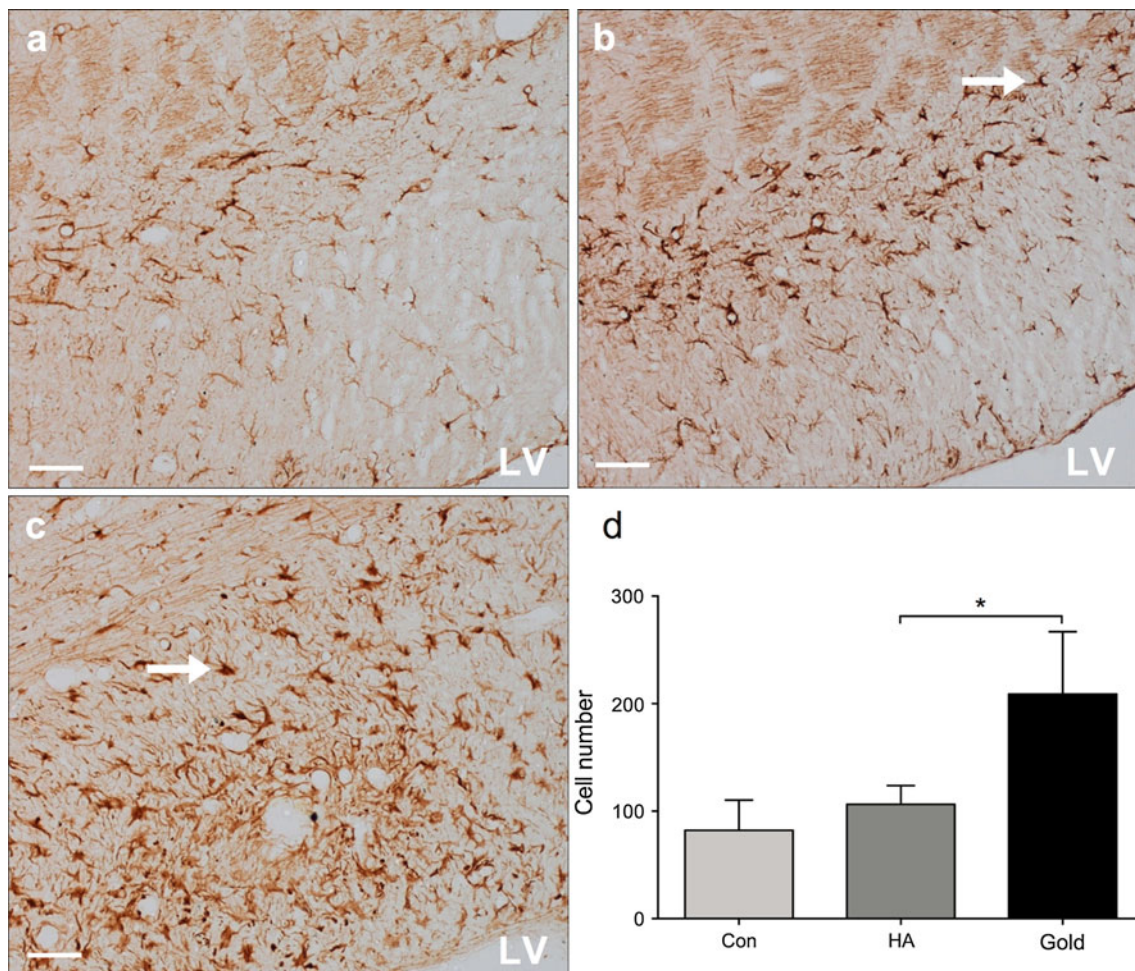


Fig. 7 Micrographs of GFAP expression above the LV, seen on the lower right, and next to the hippocampal area in a–c. a–c A marked difference in the expression of GFAP-positive cells between the vehicle- and gold-treated groups is seen (b, c, respectively). d A box

plot of the count of GFAP-positive cells, showing a significant difference between the vehicle- and gold-treated groups ($P < 0.0053$). Scale bars 50 μm

counting in highly inflamed disease loci in the brain stem revealing no difference between the gold-treated and the control groups (Fig. 4b; counting not shown). Additionally, the expression of lectin-positive cells was closely investigated to see if gold treatment had any effect on the activity and number of reactive microglia, i.e., small, round cells densely colored by lectin and located within diseased foci. Both periventricular areas above the SVZ and areas in the brain stem were evaluated (Fig. 5). No differences between treated and untreated or HA controls ($P = 0.35$) were observed.

Gold treatment reduces cell death in disease foci in the brain stem

Investigation of cell death by means of counting of TUNEL-positive cells (Fig. 6) in the brain stem showed a statistically significant reduction in gold-treated group

(11.3 ± 2.8) versus the control group (25.7 ± 5.2) ($P = 0.027$). However, comparison of the vehicle- and gold-treated groups did not reveal any statistically significant difference, although the vehicle group did not deviate significantly from the control group (21.6 ± 7.1).

Dissolucytotically released gold ions induce astrogliosis

Reactive astrocytes, displaying a high degree of disease activity, were counted in anatomically matched areas. Generally, the pathological changes were most pronounced ventrolaterally in the brain stem either close to or in heavily myelinated areas. The effect of the gold treatment on astrogliosis was investigated in two separate regions, one above the LVs, near the hippocampal area (Fig. 7), and the other in the brain stem next to the fourth ventricle (Fig. 8). Counting of reactive astrocytes showed a statistically

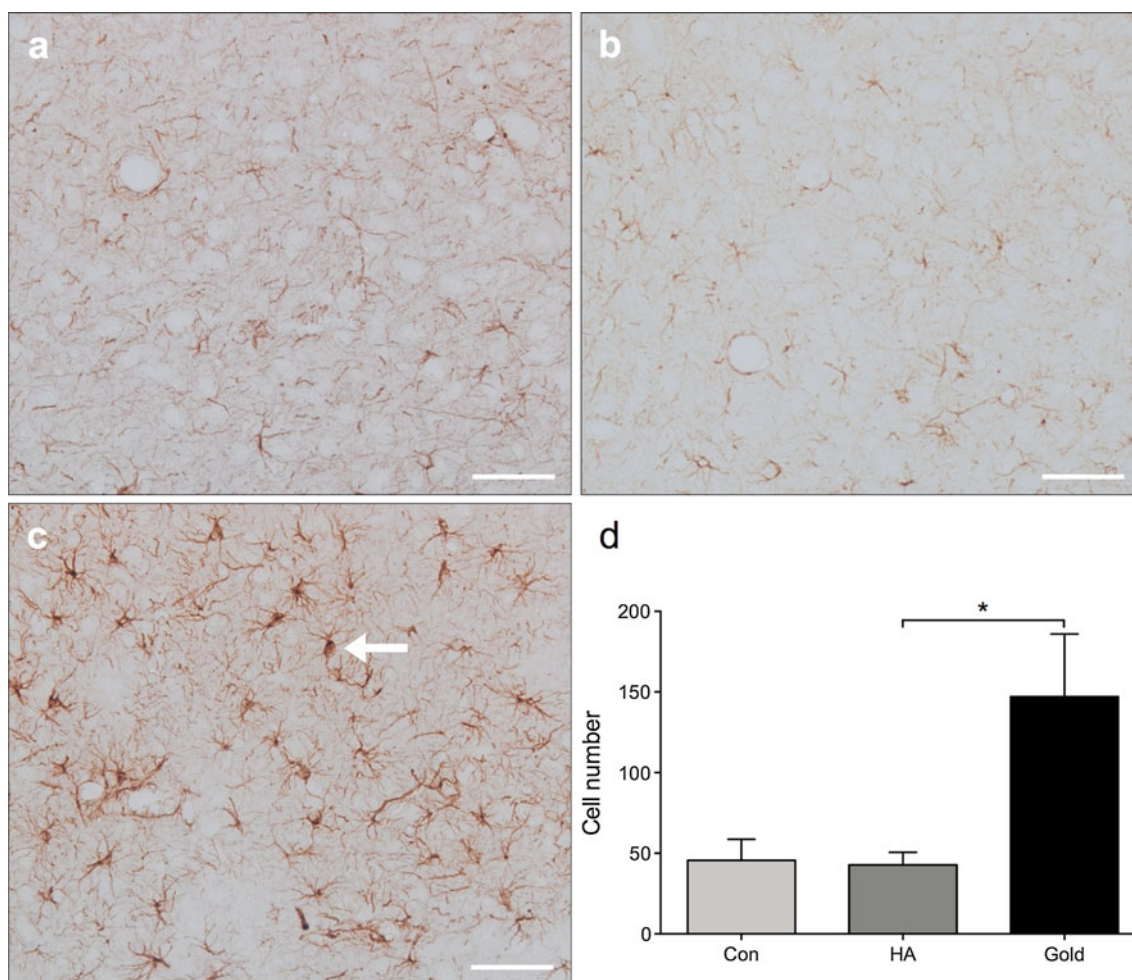


Fig. 8 Micrographs of the GFAP expression in the brain stem next to the fourth ventricle. **a–c** A clear difference between the vehicle- and gold-treated groups in **b** and **d** is seen. **d** Counting of GFAP-positive

cells can be seen in the box plot, showing a significant difference between the vehicle- and gold-treated groups ($P < 0.040$). Scale bars 50 μ m

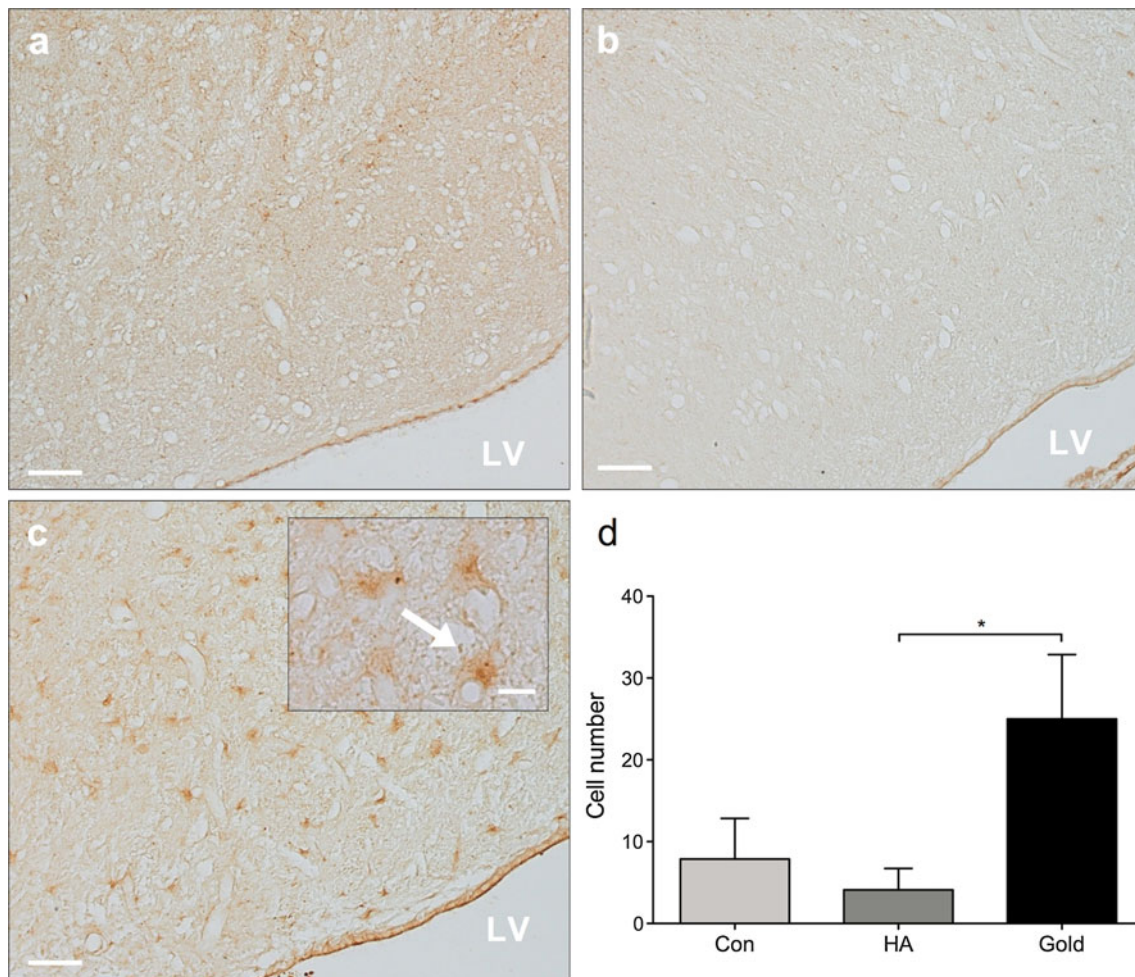


Fig. 9 Micrographs of frizzled-9 expression above the LV are seen in panel **a–c**, for the vehicle- and gold-treated groups, respectively. In the vehicle-treated group, one animal had the same level of frizzled-9-positive cells as in the gold-treated animals; the rest was totally

devoid of any expression of positive cells. **d** A marked and statistically significant increase was seen in the gold-treated animals ($P = 0.045$). Scale bars 100 μm (**a–c**) and 50 μm (inset in **c**)

significant increase ($P = 0.0053$ and $P = 0.040$) in the number of reactive astrocytes in both regions (209 ± 25.9 and 148 ± 38.9 , respectively) compared to HA-treated control animals (106.4 ± 7.7 and 42 ± 7.8 , respectively).

Dissolucytotic gold ions evokes stem cell responses as evaluated by frizzled-9 and nestin

Frizzled-9-positive cells were counted between the SVZ and CC, in areas with the highest density of positive cells. A pronounced up-regulation ($P = 0.045$) of NSCs was recorded in gold-treated animals (25 ± 7.8) compared to the vehicle control group (4.1 ± 2.6) (Fig. 9). Being a marker of NSCs (Wiese et al. 2004), nestin-positive cells were counted within two locations, in the SVZ of the LVs (Fig. 1). The two counted areas each measured $250 \times 250 \mu\text{m}$ and were placed in areas of high nestin density. The average cell count

per animal was calculated. A significant increase ($P = 0.024$) of star-shaped nestin-positive cells was seen in the gold-treated group (6.3 ± 1.8) compared to the vehicle-treated group (1.6 ± 0.9) (Fig. 10).

Metallothionein-1 and -2 is up-regulated by gold treatment

MT-1 and -2 positive cells appeared morphologically to be as reactive astrocytes, with a display of nearly completely retracted processes and a dense colored and almost round soma. The gold-treated group revealed a statistically significant increase in MT-1 and -2 positive cells (13.9 ± 1.2) compared to the vehicle-treated group (3.9 ± 2.6) ($P = 0.0045$), which displayed only a slightly higher amount of MT-1 and -2 positive cells than the EAE control animals (Fig. 11).

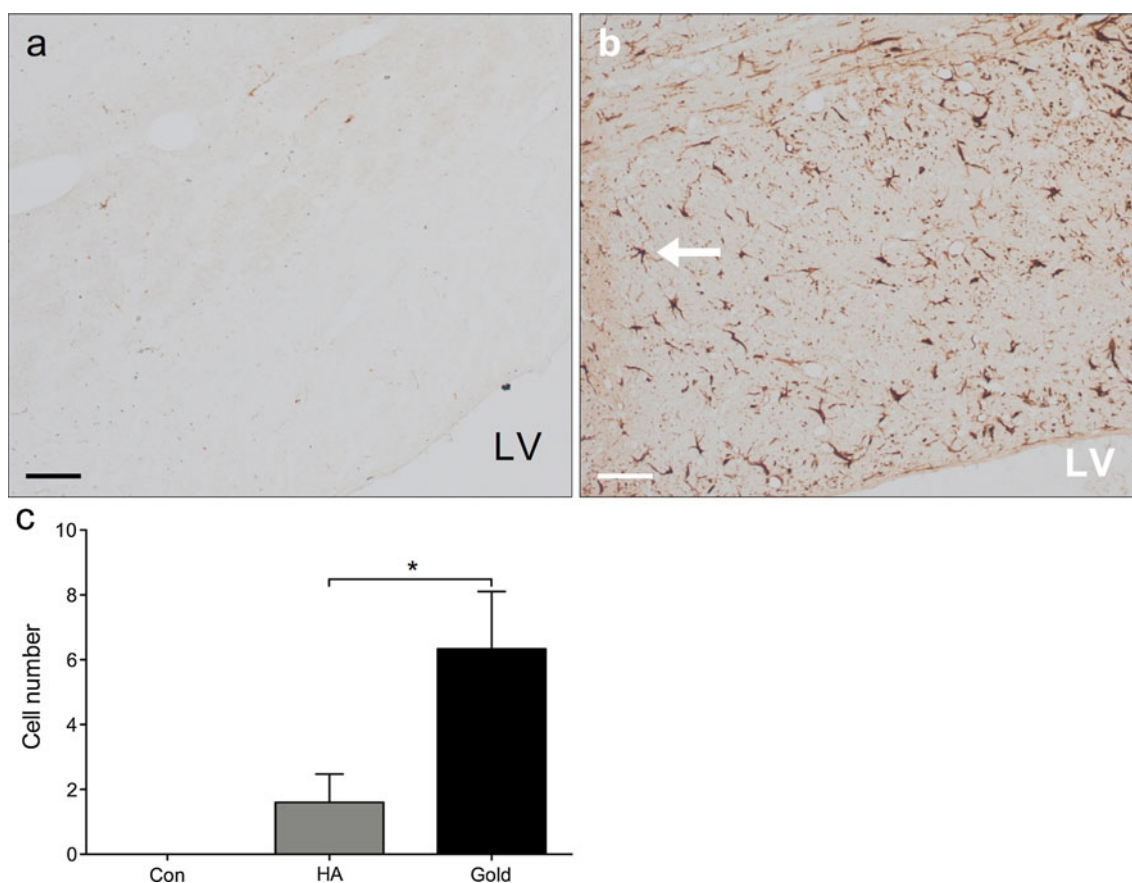


Fig. 10 Micrographs of nestin-positive staining showing cells of astrocytic morphology (**a**, **b**). Two areas measuring $250 \times 250 \mu\text{m}$ were counted in the areas above and rostrally from LV and the mean

cell count calculated. A statistically significant difference between the vehicle- and gold-treated animals was seen ($P = 0.024$). Scale bars $20 \mu\text{m}$

Discussion

This study reveals that metallic gold implants are able to actively slow down symptoms of disease progression in the MS model of experimental autoimmune encephalitis. The EAE model has been used for more than seven decades as an established model for the human disease (Gold et al. 2006), because it mirrors many of the neurological and pathological aspects of the human MS disease (Hohlfeld and Wekerle 2001).

Bio-liberated gold ions have previously been shown to ameliorate trauma-induced inflammation (Larsen et al. 2008), but the effect of dissolucytotic gold ions on an autoimmune type of inflammation has not previously been examined. The previous gold studies monitored the immunosuppressive effects of dissolucytotically released gold ions by immunohistochemical and histopathological means (Danscher and Larsen 2010), while the present study includes for the first time a reading of clinical effects of metallic gold implants in the brain.

While the gold particles in previous studies were placed within the brain tissue (Danscher 2002; Larsen et al. 2008;

Pedersen et al. 2009b), a ventricular location was chosen in the present study. From a theoretical point of view, this is an optimal way of dispersing the bio-released gold ions globally to all parts of the CNS. Furthermore, brain-infiltrating CD8⁺ T cell clones have been found to persist in the cerebrospinal fluid in MS patients for more than 5 years (Skulina et al. 2004), thus making LV an even more optimal target site of gold injection.

HA has been used as the suspension medium in prior studies from our laboratory (Larsen et al. 2008). ProVisc, a sterile 8 % hyaluronic acid used in ophthalmological surgery, was found to be suitable for suspending gold particles between 20 and 45 microns in diameter, especially due to a perfect viscosity. Natural accumulation of HA occurs in inflamed (Back et al. 2005) and ischemic brain tissue (Wang et al. 2001; Al Qteishat et al. 2006) and such accumulations might increase microglial activation (Wang et al. 2006). On the other hand, some studies indicate that HA accumulations can have regenerative properties inducing cell infiltration, angiogenesis as well as survival of neurons (Al'Qteishat et al. 2006), even though some HA forms might inhibit remyelination (Back et al. 2005).

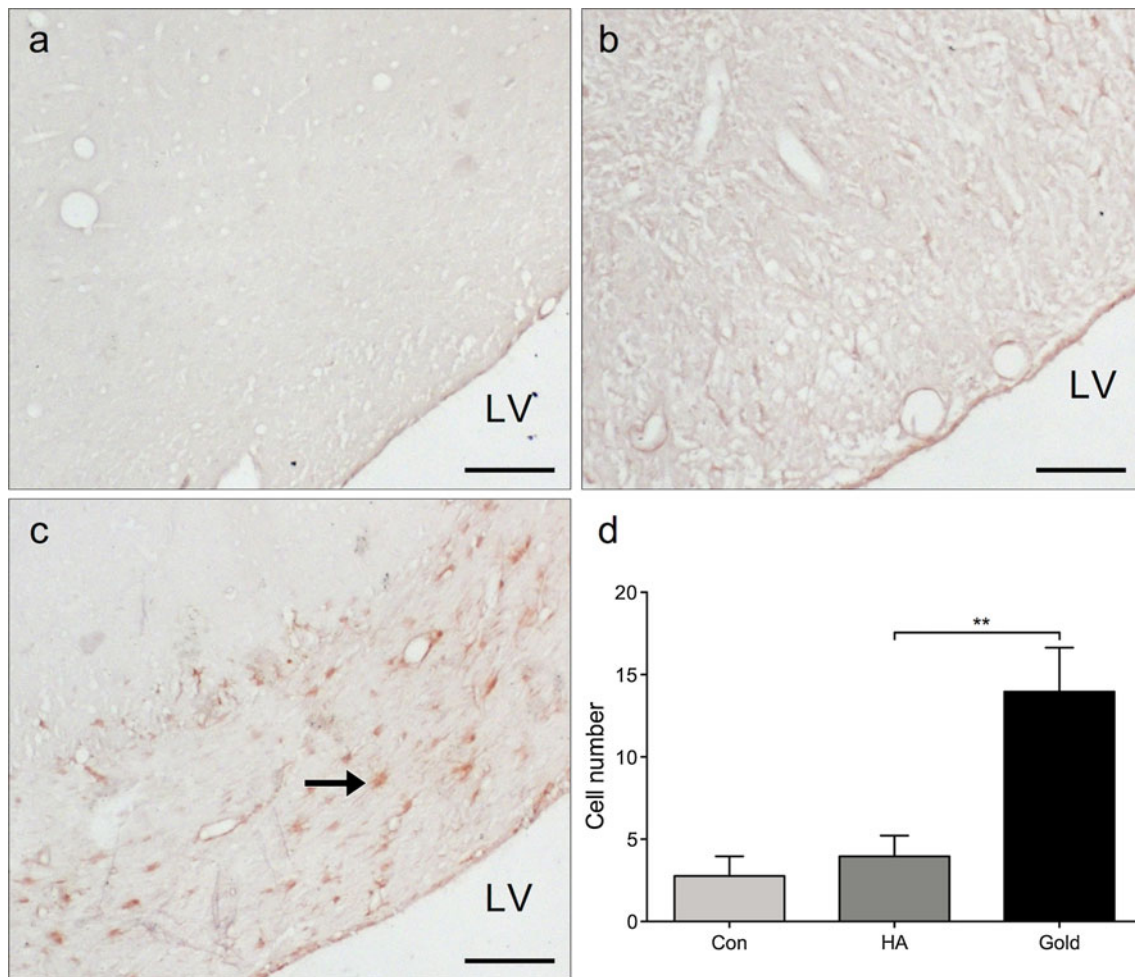


Fig. 11 Micrographs of metallothionein-1 and -2 expressions in parenchyma between the SVZ and CC above the LV are seen in panel (a–c). The arrow in c denotes an MT-1 and -2 positive cell. **d** A

marked and significant increase was seen in the gold-treated animals compared to the vehicle group ($P = 0.0045$). Scale bars 100 μm

Though it cannot be excluded that the minute amount of HA used to suspend the gold particles is capable of influencing inflammation in tissue (Bot et al. 2008; Heyworth et al. 2008; Thibeault and Dufflo 2008) all the differences found between HA controls and the gold-treated animals are so evident that the beneficial effect of the dissolucytotic gold ions is beyond any doubt. While the HA likely disappears relatively fast within the organism as there is a turnover of one-third of total body HA per day (Bot et al. 2008), the gold particles constitute a permanent gold ion reservoir that will release gold ions as long as they are present in the brain.

Morphologically, basic inflammatory responses such as microglial and lymphocyte invasion do not seem to be reduced in our setup when examining disease hot spots; however, the tendencies toward a lower clinical score as well as the significant slowing of the disease-related weight loss clearly indicate an effect of the treatment. The EAE model exhibits, as clearly seen, a high degree of disease

activity and it is possible that gold ion-induced anti-inflammatory effects would have been more obvious within the first few days of inflammation. Further studies using stereological tools might be of value in confirming anti-inflammatory effects histopathologically, although it should be kept in mind that the number of macrophages might not be as relevant as their type of inflammatory response. Recently, an increased focus has been on the IL-17 cytokine family. These cytokines are highly expressed during blood–brain barrier disruption and neuroinflammation (Jadidi-Niaragh and Mirshafiey 2011). As gold compounds are known to suppress NF- κ B (Yang et al. 1995) and as this transcriptional factor is vital for induction of most IL-17 inducible genes (Hot et al. 2011), gold-induced modulation of the IL-17 pathways might thus be a possible explanation for the clinical effects of gold treatment seen in this study. Although inflammation is present, our histopathological findings also suggest that gold ions modulate inflammation in a direction more suitable for brain repair,

displaying decrease in cell death paralleling an up-regulation of astrogliosis.

Recent years have spurred an intense debate of the role of astrocytes in MS (Sofroniew and Vinters 2010; Buffo et al. 2010; Nair et al. 2008; Seifert et al. 2006; Williams et al. 2007), and at present many authors have suggested that up-regulation of the reactive astrocytes exerts a positive effect on the disease pathology (Nash et al. 2011). Astrocytosis is also known to affect adult neurogenesis (Robel et al. 2011; Buffo et al. 2010) and the astrocytes are also the source of the neuroprotective metalloproteins metallothionein (MT-I and -2) (West et al. 2008; West et al. 2011). Exogenous treatment with Zn-MT-1 and -2 has previously been found to reduce axonal damage; and it is likely that gold-induced MT-1 and -2 contribute to the protective effects of gold treatment (Chung et al. 2008), an effect also seen in previous studies (Pedersen et al. 2010; Pedersen et al. 2009a).

Our results also support previous findings (Larsen et al. 2008) that dissolucytotically liberated gold ions can induce a neuro-regenerative response, a further indication of an altered brain environment. Stem cell response was visualized using frizzled-9, a marker specific for NSCs in the early developmental stages of CNS (Kirikoshi et al. 1999; Van Raay et al. 2001; Katoh 2008) as well as adult NSCs (Zhang et al. 2006). We found that frizzled-9-positive NSCs were up-regulated in the brain parenchyma above the SVZ in the gold-treated animals, which is indeed remarkable taking into account the amount of bio-liberated gold ions. Nestin, another marker of NSCs (Ayuso-Sacido et al. 2008; Michalczyk and Ziman 2005), was also up-regulated in the same areas.

Looking for signs of regeneration in hippocampus with the used markers, no signs of a hippocampal stem cell response was found in this study (data not shown). However, it cannot be ruled out that the gold-induced imbursement of the regenerative forces in the microenvironment in SVZ might also affect the hippocampus during longtime continuous gold treatment. Such effects would of course be extremely beneficial as the hippocampus is involved in functions such as learning, memory, anxiety and even stress regulation (Leuner and Gould 2010).

In conclusion, we found that treating EAE-immunized rats with gold particles administrated via the LVs ameliorates the clinical progression of the disease, reduces cell death, causes astrogliosis and induces the recruitment of NSCs. This holds promises for the possible clinical use of non-toxic gold compounds in a long-term treatment of neurodegenerative diseases, boosting neurogenesis and protecting against the devastating effects of recurring neuroinflammation.

Acknowledgments The authors would like to thank Albert Meier and Dorete Jensen for their excellent technical assistance. We are

grateful for the financial support from the Aarhus University Research Foundation, Danielsen Foundation, Den Lægevidenskabelige Forskningsfond and Fonden af 17.12.1981 and Lykfeldts Legat.

References

- Acarin L, Vela JM, Gonzalez B, Castellano B (1994) Demonstration of poly-*N*-acetyl lactosamine residues in ameboid and ramified microglial cells in rat brain by tomato lectin binding. *J Histochem Cytochem* 42:1033–1041
- Achiron A, Doniger GM, Harel Y, Appleboim-Gavish N, Lavie M, Simon ES (2007) Prolonged response times characterize cognitive performance in multiple sclerosis. *Eur J Neurol* 14:1102–1108
- Al Qteishat A, Gaffney JJ, Krupinski J, Slevin M (2006) Hyaluronan expression following middle cerebral artery occlusion in the rat. *NeuroReport* 17:1111–1114
- Al'Qteishat A, Gaffney J, Krupinski J, Rubio F, West D, Kumar S, Kumar P, Mitsios N, Slevin M (2006) Changes in hyaluronan production and metabolism following ischaemic stroke in man. *Brain* 129:2158–2176
- Ayuso-Sacido A, Roy NS, Schwartz TH, Greenfield JP, Boockvar JA (2008) Long-term expansion of adult human brain subventricular zone precursors. *Neurosurgery* 62:223–229 (discussion 229–231)
- Back SA, Tuohy TM, Chen H, Wallingford N, Craig A, Struve J, Luo NL, Banine F, Liu Y, Chang A, Trapp BD, Bebo BFJ, Rao MS, Sherman LS (2005) Hyaluronan accumulates in demyelinated lesions and inhibits oligodendrocyte progenitor maturation. *Nat Med* 11:966–972
- Bot PT, Hoefler IE, Piek JJ, Pasterkamp G (2008) Hyaluronic acid: targeting immune modulatory components of the extracellular matrix in atherosclerosis. *Curr Med Chem* 15:786–791
- Buffo A, Rolando C, Ceruti S (2010) Astrocytes in the damaged brain: molecular and cellular insights into their reactive response and healing potential. *Biochem Pharmacol* 79:77–89
- Caetano SC, Hatch JP, Brambilla P, Sassi RB, Nicoletti M, Mallinger AG, Frank E, Kupfer DJ, Keshavan MS, Soares JC (2004) Anatomical MRI study of hippocampus and amygdala in patients with current and remitted major depression. *Psychiatry Res* 132:141–147
- Chung RS, Penkowa M, Dittmann J, King CE, Bartlett C, Asmussen JW, Hidalgo J, Carrasco J, Leung YK, Walker AK, Fung SJ, Dunlop SA, Fitzgerald M, Beazley LD, Chuah MI, Vickers JC, West AK (2008) Redefining the role of metallothionein within the injured brain: extracellular metallothioneins play an important role in the astrocyte-neuron response to injury. *J Biol Chem* 283:15349–15358
- Danscher G (2002) In vivo liberation of gold ions from gold implants. Autometallographic tracing of gold in cells adjacent to metallic gold. *Histochem Cell Biol* 117:447–452
- Danscher G, Larsen A (2010) Effects of dissolucytotic gold ions on recovering brain lesions. *Histochem Cell Biol* 133:367–373
- Danscher G, Stoltenberg M (2006) Silver enhancement of quantum dots resulting from (1) metabolism of toxic metals in animals and humans, (2) in vivo, in vitro and immersion created zinc-sulphur/zinc-selenium nanocrystals, (3) metal ions liberated from metal implants and particles. *Prog Histochem Cytochem* 41:57–139
- Deng W, Saxe MD, Gallina IS, Gage FH (2009) Adult-born hippocampal dentate granule cells undergoing maturation modulate learning and memory in the brain. *J Neurosci* 29:13532–13542
- Doucey MA, Goffin L, Naeher D, Michielin O, Baumgartner P, Guillaume P, Palmer E, Luescher IF (2003) CD3 delta

- establishes a functional link between the T cell receptor and CD8. *J Biol Chem* 278:3257–3264
- Drachman DB, Brodsky RA (2005) High-dose therapy for autoimmune neurologic diseases. *Curr Opin Oncol* 17:83–88
- Forestier J (1934) Rheumatoid arthritis and its treatment by gold salts. *The Lancet* 224:646–648
- Ge S, Yang CH, Hsu KS, Ming GL, Song H (2007) A critical period for enhanced synaptic plasticity in newly generated neurons of the adult brain. *Neuron* 54:559–566
- Giovannoni G, Ebers G (2007) Multiple sclerosis: the environment and causation. *Curr Opin Neurol* 20:261–268
- Gold R, Linington C, Lassmann H (2006) Understanding pathogenesis and therapy of multiple sclerosis via animal models: 70 years of merits and culprits in experimental autoimmune encephalomyelitis research. *Brain* 129:1953–1971
- Gold SM, Kern KC, O'Connor MF, Montag MJ, Kim A, Yoo YS, Giesser BS, Sicotte NL (2010) Smaller cornu ammonis 2–3/dentate gyrus volumes and elevated cortisol in multiple sclerosis patients with depressive symptoms. *Biol Psychiatry* 68:553–559
- Gonzalez-Perez O, Jauregui-Huerta F, Galvez-Contreras AY (2010) Immune system modulates the function of adult neural stem cells. *Curr Immunol Rev* 6:167–173
- Heyworth BE, Lee JH, Kim PD, Lipton CB, Strauch RJ, Rosenwasser MP (2008) Hylan versus corticosteroid versus placebo for treatment of basal joint arthritis: a prospective, randomized, double-blinded clinical trial. *J Hand Surg Am* 33:40–48
- Hickey WF, Gonatas NK, Kimura H, Wilson DB (1983) Identification and quantitation of T lymphocyte subsets found in the spinal cord of the Lewis rat during acute experimental allergic encephalomyelitis. *J Immunol* 131:2805–2809
- Hohlfeld R, Wekerle H (2001) Immunological update on multiple sclerosis. *Curr Opin Neurol* 14:299–304
- Holman DW, Klein RS, Ransohoff RM (2010) The blood–brain barrier, chemokines and multiple sclerosis. *Biochim Biophys Acta* 1812:220–230
- Hot A, Zrioual S, Toh ML, Lenief V, Miossec P (2011) IL-17A-versus IL-17F-induced intracellular signal transduction pathways and modulation by IL-17RA and IL-17RC RNA interference in rheumatoid synoviocytes. *Ann Rheum Dis* 70:341–348
- Imrich H, Harzer K (2001) On the role of peripheral macrophages during active experimental allergic encephalomyelitis (EAE). *J Neural Transm* 108:379–395
- Jadidi-Niaragh F, Mirshafiey A (2011) Th17 cell, the new player of neuroinflammatory process in multiple sclerosis. *Scand J Immunol* 74:1–13
- Katoh M (2008) WNT signaling in stem cell biology and regenerative medicine. *Curr Drug Targets* 9:565–570
- Kirikoshi H, Sagara N, Koike J, Tanaka K, Sekihara H, Hirai M, Katoh M (1999) Molecular cloning and characterization of human Frizzled-4 on chromosome 11q14–q21. *Biochem Biophys Res Commun* 264:955–961
- Larsen A, Kolind K, Pedersen DS, Doering P, Pedersen MO, Danscher G, Penkowa M, Stoltenberg M (2008) Gold ions bio-released from metallic gold particles reduce inflammation and apoptosis and increase the regenerative responses in focal brain injury. *Histochem Cell Biol* 130:681–692
- Leuner B, Gould E (2010) Structural plasticity and hippocampal function. *Annu Rev Psychol* 61(111–40):C1–C3
- Love S, Louis DN, Ellison DW (2008) Greenfield's neuropathology, 8th edition (2 volume set) (Hodder Arnold Publication). Oxford University Press, New York
- McFarland HF, Martin R (2007) Multiple sclerosis: a complicated picture of autoimmunity. *Nat Immunol* 8:913–919
- Michalczyk K, Ziman M (2005) Nestin structure and predicted function in cellular cytoskeletal organisation. *Histol Histopathol* 20:665–671
- Nair A, Frederick TJ, Miller SD (2008) Astrocytes in multiple sclerosis: a product of their environment. *Cell Mol Life Sci* 65:2702–2720
- Nash B, Ioannidou K, Barnett SC (2011) Astrocyte phenotypes and their relationship to myelination. *J Anat* 219:44–52
- Olson DP, Dombkowski DM, Kelliher AS, Pontillo C, Anderson DC, Pfeffer FI (2004) Differential expression of cell surface antigens on subsets of CD4+ and CD8+ T cells. *Med Sci Monit* 10:BR39–BR45
- Paxinos G, Watson C (1986) The rat brain in stereotaxic coordinates. Academic Press, London
- Pedersen MO, Larsen A, Pedersen DS, Stoltenberg M, Penkowa M (2009a) Metallic gold treatment reduces proliferation of inflammatory cells, increases expression of VEGF and FGF, and stimulates cell proliferation in the subventricular zone following experimental traumatic brain injury. *Histol Histopathol* 24:573–586
- Pedersen MO, Larsen A, Pedersen DS, Stoltenberg M, Penkowa M (2009b) Metallic gold reduces TNF α expression, oxidative DNA damage and pro-apoptotic signals after experimental brain injury. *Brain Res* 1271:103–113
- Pedersen MO, Larsen A, Stoltenberg M, Penkowa M (2010) Bio-released gold ions modulate expression of neuroprotective and hematopoietic factors after brain injury. *Brain Res* 1307:1–13
- Robel S, Berninger B, Gotz M (2011) The stem cell potential of glia: lessons from reactive gliosis. *Nat Rev Neurosci* 12:88–104
- Schiff MH, Whelton A (2000) Renal toxicity associated with disease-modifying antirheumatic drugs used for the treatment of rheumatoid arthritis. *Semin Arthritis Rheum* 30:196–208
- Seifert G, Schilling K, Steinhauser C (2006) Astrocyte dysfunction in neurological disorders: a molecular perspective. *Nat Rev Neurosci* 7:194–206
- Sicotte NL, Kern KC, Giesser BS, Arshanapalli A, Schultz A, Montag M, Wang H, Bookheimer SY (2008) Regional hippocampal atrophy in multiple sclerosis. *Brain* 131:1134–1141
- Skulina C, Schmidt S, Dornmair K, Babbe H, Roers A, Rajewsky K, Wekerle H, Hohlfeld R, Goebels N (2004) Multiple sclerosis: brain-infiltrating CD8+ T cells persist as clonal expansions in the cerebrospinal fluid and blood. *Proc Natl Acad Sci USA* 101:2428–2433
- Sofroniew MV, Vinters HV (2010) Astrocytes: biology and pathology. *Acta Neuropathol* 119:7–35
- Thibeault SL, Duffo S (2008) Inflammatory cytokine responses to synthetic extracellular matrix injection to the vocal fold lamina propria. *Ann Otol Rhinol Laryngol* 117:221–226
- Trapp BD, Nave KA (2008) Multiple sclerosis: an immune or neurodegenerative disorder? *Annu Rev Neurosci* 31:247–269
- Van Raay TJ, Wang YK, Stark MR, Rasmussen JT, Francke U, Vetter ML, Rao MS (2001) Frizzled 9 is expressed in neural precursor cells in the developing neural tube. *Dev Genes Evol* 211:453–457
- Wang H, Zhan Y, Xu L, Feuerstein GZ, Wang X (2001) Use of suppression subtractive hybridization for differential gene expression in stroke: discovery of CD44 gene expression and localization in permanent focal stroke in rats. *Stroke* 32:1020–1027
- Wang MJ, Kuo JS, Lee WW, Huang HY, Chen WF, Lin SZ (2006) Translational event mediates differential production of tumor necrosis factor- α in hyaluronan-stimulated microglia and macrophages. *J Neurochem* 97:857–871
- West AK, Hidalgo J, Eddins D, Levin ED, Aschner M (2008) Metallothionein in the central nervous system: roles in protection, regeneration and cognition. *Neurotoxicology* 29:489–503
- West AK, Leung JY, Chung RS (2011) Neuroprotection and regeneration by extracellular metallothionein via lipoprotein-receptor-related proteins. *J Biol Inorg Chem* 16:1115–1122

- Wiese C, Rolletschek A, Kania G, Blyszczuk P, Tarasov KV, Tarasova Y, Wersto RP, Boheler KR, Wobus AM (2004) Nestin expression—a property of multi-lineage progenitor cells? *Cell Mol Life Sci* 61:2510–2522
- Williams HJ (1935) Prevention of severe reactions in the gold treatment of rheumatoid arthritis. *Br Med J* 2:1098
- Williams A, Piaton G, Lubetzki C (2007) Astrocytes—friends or foes in multiple sclerosis? *Glia* 55:1300–1312
- Wisikin AE, Davies JH, Wootton SA, Beattie RM (2010) Energy expenditure, nutrition and growth. *Arch Dis Child* 96:56–72
- Zhang Z, Schittenhelm J, Guo K, Buhring HJ, Trautmann K, Meyermann R, Schluesener HJ (2006) Upregulation of frizzled 9 in astrocytomas. *Neuropathol Appl Neurobiol* 32:615–624